JOURNAL OF SPACECRAFT AND ROCKETS
Vol. 42, No. 2, March–April 2005

Aerodynamic Performances of Lifting-Body Configurations for a Reentry Vehicle

Hiroshi Kawato,* Shigeya Watanabe,† Yukimitsu Yamamoto,‡ and Kenji Fujii§
National Aerospace Laboratory, Tokyo 182-8522, Japan

Aerodynamic characteristics of four lifting-body-type configurations for a reentry vehicle, namely, a baseline configuration, a fin-off configuration, a 45-deg canted fin configuration and an upswept upper-aftbody configuration, are investigated by wind-tunnel tests and compared, focusing on aerodynamic performance aspects such as longitudinal trim capability, longitudinal and lateral/directional static stability, and subsonic lifting surface loading. The upswept upper-aftbody configuration showed the best performance from longitudinal trim, and longitudinal and lateral/directional static stability points of view, which suggests that modifying the upper aft part of the fuselage of the baseline configuration is the most promising approach to improving its characteristics.

Nomenclature

b	=	vehicle span, m
CAF	=	forebody axial-force coefficient
CD	=	drag coefficient
CDF	=	forebody drag coefficient
$CD0$	=	minimum drag coefficient
CL	=	lift coefficient
Cl	=	rolling-moment coefficient
Cm	=	pitching-moment coefficient
Cn	=	yawing-moment coefficient
$Cn\beta dyn$	=	dynamic directional stability coefficient, 1/deg
CY	=	side-force coefficient
Izz/Ixx	=	ratio of moment of inertia around z and x axes
LB	=	fuselage length, m
M	=	freestream Mach number
S	=	fuselage planform area, m^2
W	=	vehicle weight, kg
W/CLS	=	lifting surface loading, kg/m^2
Xcg	=	center of gravity, origin at the nose
Xcp/LB	=	center of pressure normalized by LB, origin at the nose
Xnp/LB	=	longitudinal neutral point normalized by LB, origin at the nose
Xnp,y_dyn	=	lateral/directional neutral point normalized by LB, origin at the nose
α	=	angle of attack, deg
β	=	sideslip angle, deg
δe	=	elevator deflection angle, deg
ε	=	emissivity

Subscripts

α	=	angle-of-attack derivatives
β	=	side-slip-angle derivatives

Introduction

A NUMBER of studies into reusable space transportation systems to afford safer and cheaper access to space are being carried out around the world. However, the technologies required for such systems are state of the art, and their development is costly and risky, necessitating a step-by-step approach to development with a number of flight experiments or technology demonstrators.

Japan has successfully conducted a series of subscale flight experiments to acquire reentry technologies for reusable space transportation systems: the orbital reentry experiment,[1] the hypersonic flight experiment (HYFLEX),[2] and the automatic landing experiment.[3] A high-speed flight demonstration experiment will also be conducted to complement the speed range covered by the previous experiments.[4] However, each of these experiments covered only a limited range of reentry flight conditions, and the vehicle configurations were somewhat optimized to the specific experimental objectives. A demonstration covering the whole reentry flight phase with a single vehicle configuration is therefore necessary as the next step toward the development of a reusable space transportation system.

The National Aerospace Laboratory of Japan (NAL) is conducting a feasibility study on demonstrating total reentry technology using a single vehicle configuration.[5] In this study, a vehicle is launched into low Earth orbit by an H-IIA rocket inside an off-the-shelf payload fairing. After completing a single orbit, it deorbits and reenters the atmosphere, decelerates to subsonic speed, and lands softly with a parachute or a parafoil and an airbag (Fig. 1).[5] Because the vehicle size is severely constrained by the payload fairing, a lifting-body-type configuration is considered more appropriate than a wing-body configuration because of its volumetric efficiency and aeroheating characteristics.

Although various lifting-body-type vehicles, such as the M2-F series, the X-24 series, and the HL-10, HL-20, X-33, and X-38, have been investigated,[6] the aerodynamic design methods and the knowledge of aerodynamic characteristics at subsonic, transonic, and supersonic speeds of lifting-body configurations are not as mature as those for wing-body configurations, which have been thoroughly investigated through the design processes and lessons learned in the HOPE-X[7] and U.S. space shuttle[8] programs. Wind-tunnel tests have therefore been conducted to investigate the aerodynamic characteristics of lifting-body-type configurations in the subsonic to supersonic speed range and to accumulate knowledge and experience in their aerodynamic design.[9]

Presented as Paper 2002-5265 at the AIAA/AAAF 11th International Space Planes and Hypersonic Systems and Technologies Conference, Orleans, France, 29 September–4 October 2002; received 13 May 2003; revision received 21 April 2004; accepted for publication 27 April 2004.

*Senior Researcher, Space Transportation Project Center, 7-44-1, Jindaiji-Higashi-Machi, Chofu. Member AIAA.

†Group Leader, Space Transportation Project Center, 7-44-1, Jindaiji-Higashi-Machi, Chofu. Member AIAA.

‡Group Leader, CFD Technology Center, 7-44-1, Jindaiji-Higashi-Machi, Chofu. Member AIAA.

§Group Leader, Space Transportation Project Center, 7-44-1, Jindaiji-Higashi-Machi, Chofu.

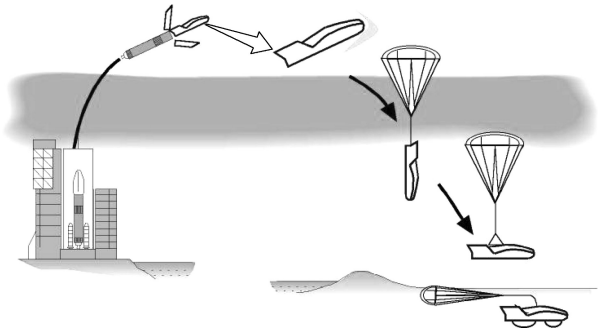

Fig. 1 Concept of the demonstration.

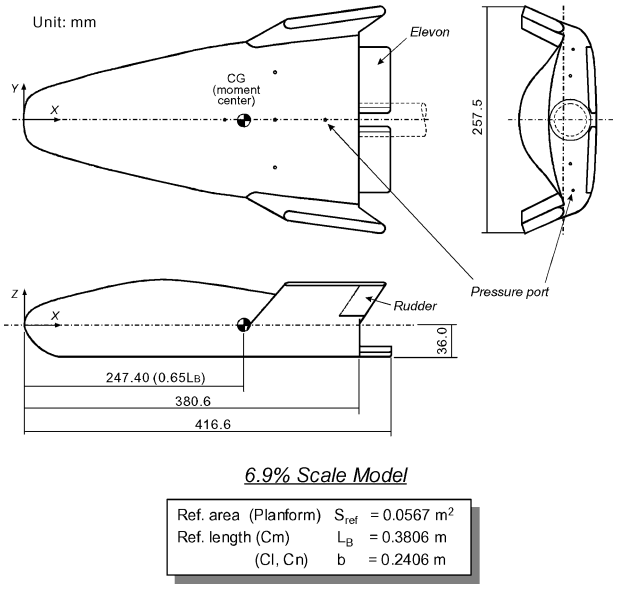

Fig. 2 Baseline configuration (6.9% scale wind-tunnel model).

The present study investigates the aerodynamic characteristics of four lifting-body configurations by wind-tunnel tests, focusing on aerodynamic performance aspects such as longitudinal trim capability, longitudinal and lateral/directional static stability, and subsonic lift or lifting surface loading.

Vehicle Configuration

Baseline Configuration

Figure 2 shows the baseline configuration for the present study. This consists of low-aspect-ratio fuselage with a relatively flat undersurface and a blunt base. The upper surface of the fuselage is raised like an airfoil, with its maximum height located at around 40% of the fuselage length. Two outboard fins, canted 20 deg outward, are mounted on upper-aft portion of the fuselage. These have a thick flat-plate cross section with cylindrical leading and trailing edges.

The baseline configuration is based on the HYFLEX vehicle, which flew in a suborbital hypersonic lifting flight experiment in 1996. The fuselage length of 5.50 m is determined by the requirement that the vehicle be housed within a 4/4D-L payload fairing for dual launch by the NASDA H-IIA launcher. The nearly triangular vehicle planform shape tends to cause the fuselage's volumetric center to be noncoincident with the center of gravity. This was compensated by tapering the upper-aft portion of the fuselage down towards the vehicle's base as shown in the side view in Fig. 2. This has the additional advantage of reducing base drag in subsonic to low supersonic flight.

The nose radius is determined from the maximum allowable heating rate (600 kW/m^2 assuming $\varepsilon = 0.78$) based on the maximum temperature sustainable by the carbon/carbon composite material (1650°C), which is to be applied to the nose of the actual vehicle.

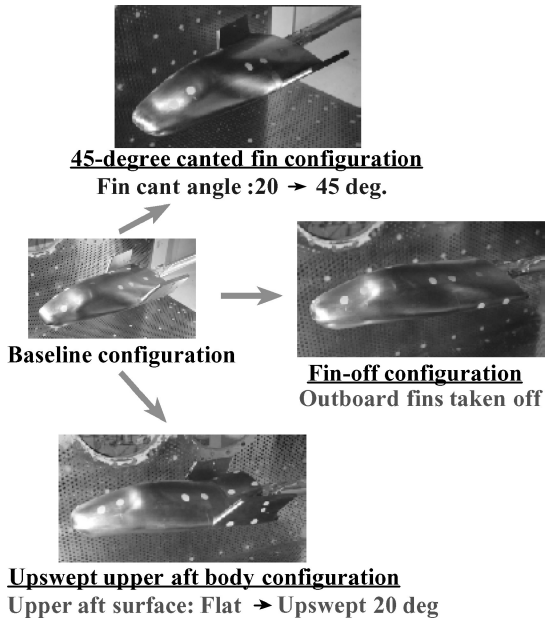

Fig. 3 Derived configurations.

The fins are toed in and canted to increase the effectiveness of the fins and rudders. Similarly to the nose radius, the radius of the fin leading edges is determined based on the maximum allowable heating rate (1400°C, $\varepsilon = 0.83$) of the medium-density ceramic tile, which is to be applied to the leading edges.

Two control surfaces (elevons) are attached at base of the fuselage, their lower surfaces contoured to the lower aft surface of the fuselage when undeflected. The elevons deflect from −20 to +20 deg and operate collectively as elevators and differentially as ailerons for longitudinal trim and pitch/roll control, producing slight yawing moment caused by the dihedral of the fuselage lower surface. A rudder is located at the trailing edge of each fin. The rudders operate mainly for yaw control and generating a slight rolling moment.

Derived Configurations

The present study also investigates three configurations derived from the baseline as shown in Fig. 3, namely, a fin-off configuration, a 45-deg canted fin configuration and an upswept upper-aftbody configuration, which has a 20-deg upswept upper aftbody (like an upward deflected body flap). The fin-off configuration was chosen to study the effect of the fins and to acquire data for fin sizing. The 45-deg canted fin configuration was chosen to study the effect of greater fin cant angle, which was expected to improve longitudinal static stability. The upswept upper-aftbody configuration was chosen to study the effect of modifying the upper surface of the fuselage. Computational-fluid-dynamics (CFD) studies had indicated that this modification should improve the trim capability of the baseline configuration.

Wind-Tunnel Tests

Wind Tunnels

Wind tunnel tests for the present study were conducted using NAL's 2 m × 2 m Transonic Wind Tunnel and 1 m × 1 m Supersonic Wind Tunnel. TWT1 is a closed-circuit, variable density transonic tunnel with a porous test section wall that covers a Mach-number range of 0.1–1.4. SWT1, an intermittent blowdown tunnel, covers a Mach-number range of 1.4–4.0 with a duration of up to 40 s. Tests were conducted at Mach 1.4 in both tunnels to check the data consistency between the two tunnels.

Models

The baseline configuration (Fig. 2) and its derivatives (Fig. 3) were tested in both tunnels using 6.9% scale models made primarily of stainless steel (SUS303). Roughness for boundary-layer transition was not used in these tests.

The models were supported at the fuselage base by either a straight sting for transonic tests, as shown in Fig. 3, or a 10-deg-deflected sting for supersonic tests. The diameter of both stings was 38 mm near the model.

Four surface-pressure ports were set at the fuselage base in order to estimate the forebody drag *CDF* or forebody axial force *CAF* from the balance output. A further five pressure ports were located at the upper-aft surface of the body to investigate the condition of the boundary layer, which was expected to separate at relatively low angles of attack, as well as to acquire data for validation of the CFD predictions.

Measurements

Six components of force and moment were measured by internal force balances installed in the models. The measured forces and moments were normalized by freestream dynamic pressure, fuselage planform area S, and reference lengths LB or b into aerodynamic coefficients, mainly in body axes and partially in stability axes.

In the transonic tests, surface-pressure measurements were made on the upper-aft fuselage and the fuselage base by a 48-port S2-type scanivalve with a Statham 10-psid differential-type pressure transducer, located in the strut that controlled the model's attitude. Pressure was measured in the supersonic tests by 10 separate pressure transducers (Druck 15 psid differential-type PDCR sensors) directly connected to each pressure port.

Observations were conducted from the side of the model using a rainbow-color schlieren system in order to investigate shock and expansion wave structure, boundary-layer separation, and vortices generated by the fuselage or fins. Images were recorded by a photographic still camera and a VHS video recorder for the supersonic tests, and by a VHS video recorder for the transonic tests.

Oil flow visualizations were conducted at several transonic test conditions to investigate the flow pattern on the upper surface of the fuselage and to gain better understanding of phenomena.

Test Conditions

The transonic tests were conducted over a Mach-number range of 0.5–1.4, whereas the supersonic tests covered a range of 1.4–4.0. Angle of attack α ranged from -7.5 to 20 deg for the transonic tests and -5 to 25 deg for the supersonic tests. These ranges were determined to cover both the angle for minimum drag *CD*0 and the maximum angle expected during actual flight. Sideslip angles β of 0 and 5 deg were tested in both the transonic and supersonic tests. Derivatives of the lateral and directional aerodynamic coefficients were calculated from values at $\beta = 0$ and 5 deg, assuming linearity of the coefficients in the β range.

Test Results for the Baseline Configuration

This section describes briefly the results from the wind-tunnel tests for the baseline configuration at subsonic to supersonic speeds.

Lift coefficients *CL*, drag coefficients *CD*, and pitching-moment coefficients *Cm* of the baseline configuration from subsonic to supersonic speeds are shown in Figs. 4–6, respectively. With increasing angle of attack, lift-curve slope *CL*α steeply decreases at around $\alpha = 5$ deg at $M = 0.5$ and 0.9, although no such apparent kink of the *CL* curve is observed for supersonic Mach numbers. Similar phenomena can be observed *CD* and *Cm* curves.

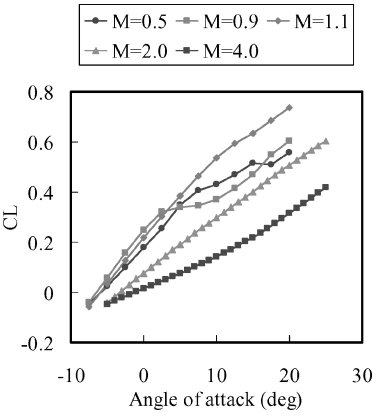

Fig. 4 Lift coefficient of the baseline configuration.

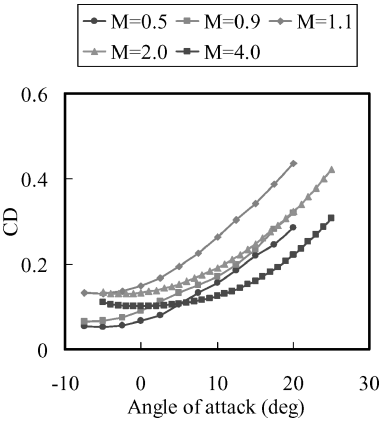

Fig. 5 Drag coefficient of the baseline configuration.

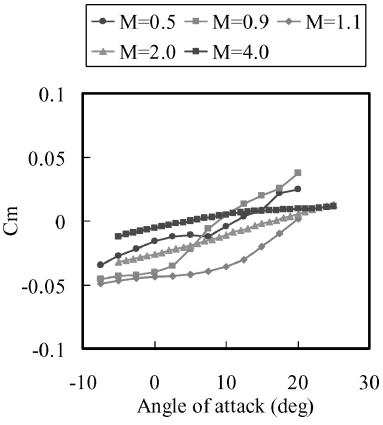

Fig. 6 Pitching-moment coefficient of the baseline configuration.

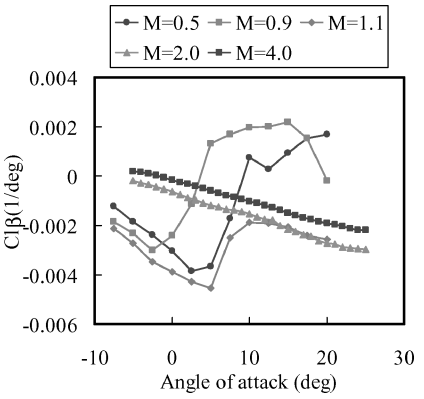

Fig. 7 Rolling-moment coefficient of the baseline configuration.

Figures 7 and 8 show derivatives of lateral and directional characteristic coefficients for the baseline configuration in terms of sideslip angle β over a Mach-number range of 0.5–4.0. In these figures, *Cl*β and *Cn*β denote rolling- and yawing-moment coefficients derivatives, respectively.

At Mach 2.0 and above, *Cl*β decreases nearly monotonically to larger negative values with increasing angle of attack because the dihedral effect of the fuselage lower/side surface and the canted fins stabilize the roll motion. Also, *Cn*β changes relatively smoothly with change of angle of attack. On the other hand, at Mach 1.1 and below, with increasing angle of attack, *Cl*β suddenly changes its behavior and move toward positive or unstable values at α between -3 and 5 deg, although at the same angle of attack *Cn*β starts decreasing in the directionally unstable direction. Note that the angles of attack for these characteristic changes almost correspond to those for the *CL* kink at $M = 0.5$ and 0.9. (Strictly, about 5 deg lower,

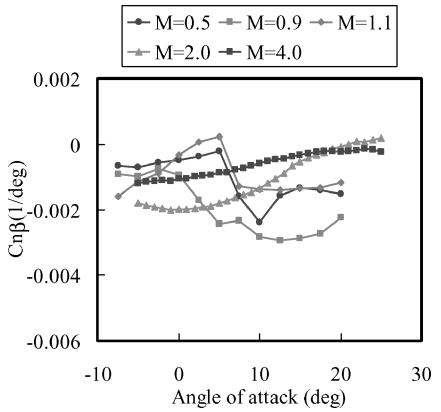

Fig. 8 Yawing-moment coefficient of the baseline configuration.

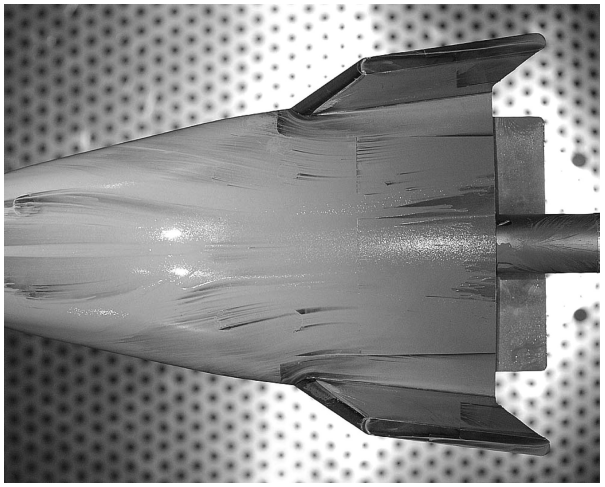

Fig. 9 Oil flow for the baseline configuration at $M = 0.5$, $\alpha = 0$ deg, and $\beta = 0$ deg.

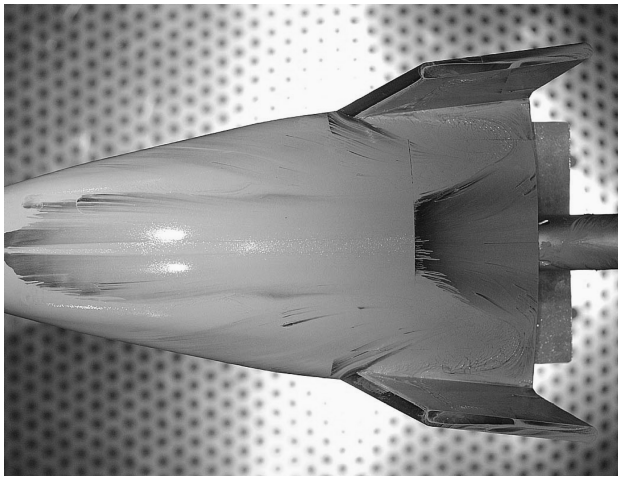

Fig. 10 Oil flow for the baseline configuration at $M = 0.5$, $\alpha = 10$ deg, and $\beta = 0$ deg.

however, this is caused by the differences in β of 0 and 5 deg.) The nonlinear lateral/directional characteristics are thus considered to have the same causes as the longitudinal nonlinear characteristics.

Figures 9 and 10 show oil flows on the upper surface of the baseline configuration at $M = 0.5$ at angles of attack of 0 and 10 deg, respectively. At $\alpha = 0$ deg the flow is rather smooth over the entire upper surface of the fuselage, but at $\alpha = 10$ deg flow separation or vortex-like flow can be observed near the roots of the fins. This seems to be one of the major causes of the just-mentioned nonlinear characteristics.

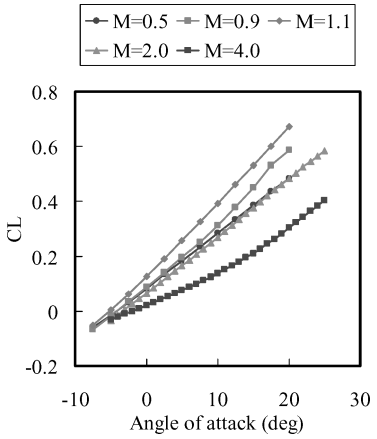

Fig. 11 Lift coefficient of the fin-off configuration.

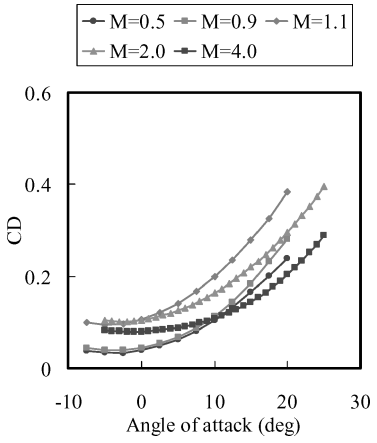

Fig. 12 Drag coefficient of the fin-off configuration.

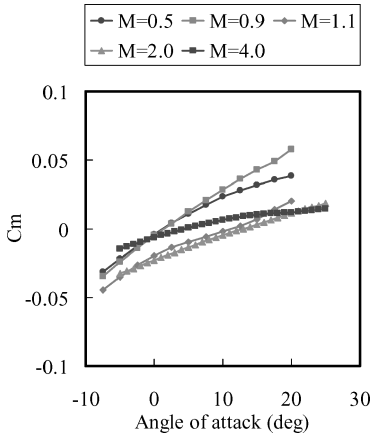

Fig. 13 Pitching-moment coefficient of the fin-off configuration.

The reason for these flow characteristics can be estimated from the results of the fin-off configuration (Figs. 11–15), which show that its aerodynamic characteristics are rather linear compared to those of the baseline. It therefore appears that the twin outboard fins make the flow on the fuselage upper surface unstable, either by their shape, location or both, causing the observed nonlinear characteristics.

Note that the fin-off configuration has lower lift than the baseline and its lateral/directional stability is rather poor at low angles of attack, so that eliminating the fins might not be the best means of improving the baseline. Improving the baseline thus requires that its aerodynamic performance and the effects of modifications be investigated as a whole.

Comparison of Aerodynamic Performance

Longitudinal Trim Capability and Static Stability

Figure 16 shows the relationship between longitudinal trim capability or the location of the center of pressure normalized by fuselage

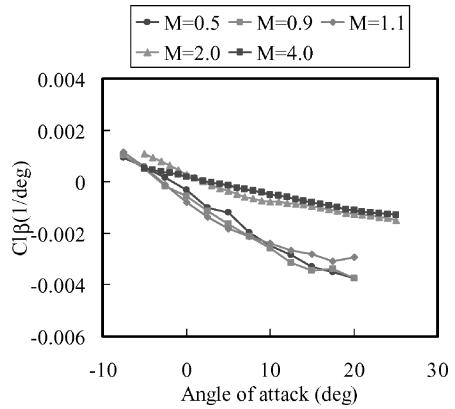

Fig. 14 Rolling-moment coefficient of the fin-off configuration.

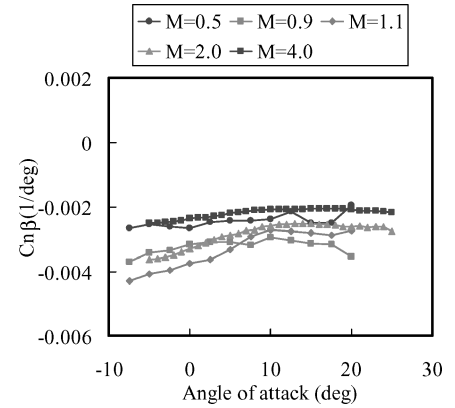

Fig. 15 Yawing-moment coefficient of the fin-off configuration.

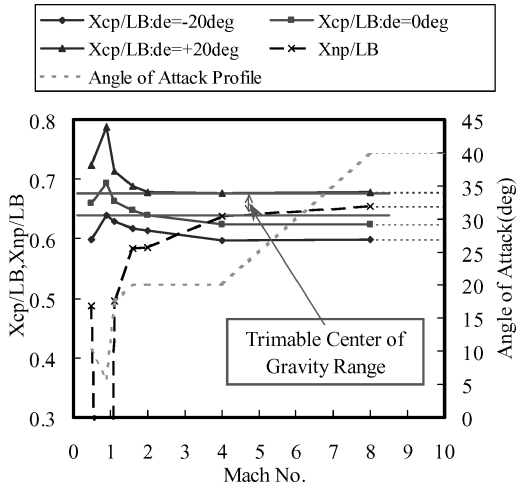

Fig. 16 Longitudinal trim capability and static stability of the baseline configuration.

length, *Xcp/LB* (origin at the nose, aft positive, as defined in Fig. 2) and static stability or neutral point normalized by the fuselage length *Xnp/LB* (origin at the nose, aft positive, as defined in Fig. 2) for the baseline configuration with varying Mach number at nominal angles of attack. Some data for elevon deflection angles (δe) of −20 and 20 deg were not acquired in the wind-tunnel tests, and these are instead estimated from body flap deflection data for the HOPE-X configuration derived from wind-tunnel tests.[10] Also, the hypersonic characteristics were estimated based on Newtonian impact theory. Nominal α profile, also shown in Fig. 16, was selected to attain the widest trimable range of center of gravity. Although the Mach-number range shown in Fig. 16 is only up to 8, it should well represent the whole flight range because aerodynamic characteristics are essentially constant over the hypersonic speed range and the angle of attack is kept constant at those speeds.

Figure 16 indicates that the baseline configuration has narrow trimable range of c.g. throughout the flight Mach-number range, assuming that the δe range for trim is bounded in the range −20 to 20 deg. Note, however, that this might not be true if the α profile is restricted because of other requirements or constraints. *Xnp/LB*, which indicates the longitudinal static stability (stable when aft of c.g.), is located forward of the trimable center-of-gravity range over most of the Mach-number range, leading to a conflict between the requirements to maintain both trim and static stability.

Figure 17 shows the relationship between longitudinal trim capability and static stability for the 45-deg canted-fin configuration with varying Mach number at nominal angles of attack. This adjustment to the cant angle of the baseline configuration from 20 to 45 deg was intended to improve static stability by shifting the neutral point aft. Comparing with Fig. 16, it can be seen that neutral point of the 45-deg canted-fin configuration is about 0.03 aft compared to the baseline configuration. However the trimable center-of-gravity range is also moved aft compared to the baseline configuration. Consequently, the neutral point is forward of the trimable center-of-gravity range over most of the Mach-number range, and so the 45-deg canted-fin modification does not improve the longitudinal static stability of the baseline configuration.

Figure 18 shows relationship between longitudinal trim capability and static stability for the fin-off configuration with varying Mach number at nominal angles of attack. Comparing with Fig. 16 for the baseline configuration, the fin-off configuration has better trim

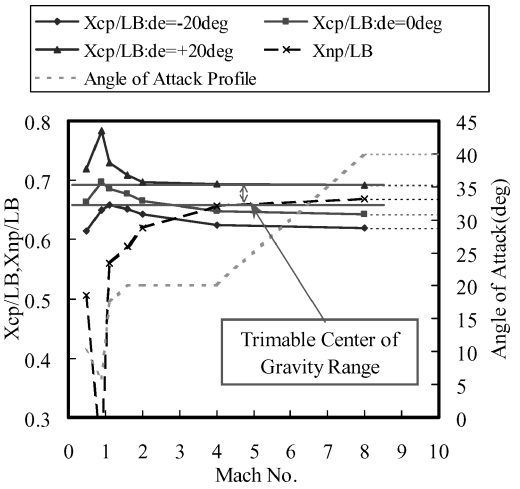

Fig. 17 Longitudinal trim capability and static stability of the 45-deg canted-fin configuration.

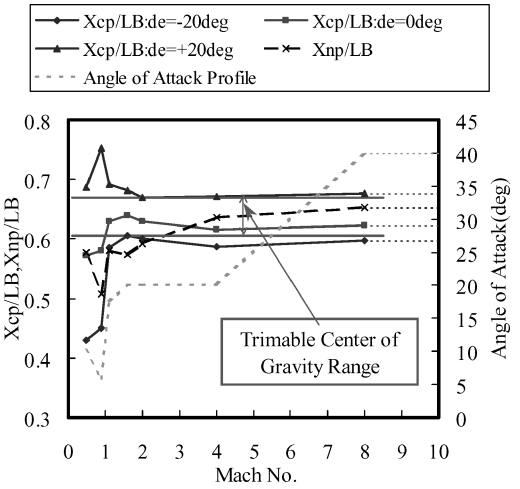

Fig. 18 Longitudinal trim capability and static stability of the fin-off configuration.

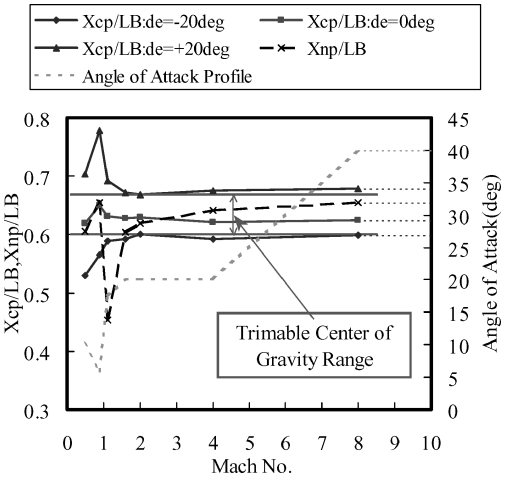

Fig. 19 Longitudinal trim capability and static stability of the upswept upper-aftbody configuration.

capability or a wider trimable center-of-gravity range. This is mainly because of the forward shift of center of pressure at transonic speed by reduced lift at the upper-aft portion of the fuselage of the fin-off configuration. The neutral point is forward of the trimable center-of-gravity range below $M = 3$.

The preceding discussions suggest that canting the fins further outboard seems not to contribute to longitudinal static stability but rather makes the current lifting-body configuration rather unstable, and that although the stability of the fin-off configuration is still insufficient it seems rather favorable from longitudinal trim and stability points of view. However, the outboard fins do contribute to lift and lateral/directional stability, as will be described later in this paper, and so an alternative means of improving the longitudinal stability of the baseline is desirable.

Figure 19 shows the relationship between longitudinal trim capability and static stability of the upswept upper-aftbody configuration at nominal angles of attack with varying Mach number. Comparing with Fig. 16 for the baseline configuration, the upswept upper-aftbody configuration has better trim capability or a wider trimable center-of-gravity range. The neutral point has shifted aft compared to the baseline configuration and is within the trimable center-of-gravity range over most of the flight Mach-number range. Therefore, the longitudinal stability of the upswept upper-aftbody configuration is much improved compared to the baseline configuration and can mostly meet the requirement to maintain both trim and static stability.

The upward deflection of the upper-aft surface is most effective for longitudinal trim capability as well as stability, mainly because of the following reasons. The longitudinal instability of the baseline configuration at low Mach numbers is caused not only by the forward location of the neutral point but also the relatively aft location of the trimable center of gravity range. As can be seen from Fig. 16, the trimable center-of-gravity range of the baseline configuration is pushed aft by the aft location of the center of pressure at transonic and low supersonic speeds. Therefore, the most effective approach to resolve the longitudinal instability of the baseline configuration is to make larger forward shift of center of pressure and larger aft shift of the neutral point, at low Mach numbers. Because the upward deflection of the upper aft surface, which shifts the center of pressure forward, is a modification on the aft portion of the leeward side, it is more effective at lower Mach numbers and lower angles of attack and has virtually no effect at high angles of attack on hypersonic speeds. Furthermore, because the upward deflection of the upper-aft surface is more effective at lower angles of attack, the pitching-moment curve slope $Cm\alpha$ decreases, especially at low angles of attack. It can be seen by comparing Fig. 20, which shows the Cm of the upswept upper-aftbody configuration, with Fig. 6. Therefore, the upward deflection of the upper-aft surface is favorable in terms of improving both center of pressure and neutral point for the baseline configuration.

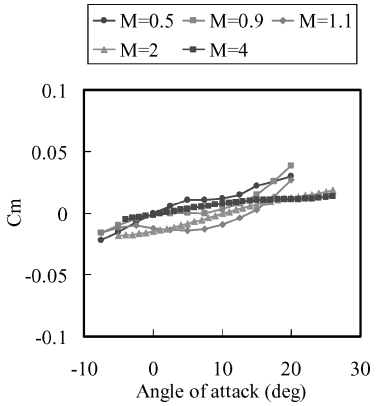

Fig. 20 Pitching-moment coefficient of the upswept upper-aftbody configuration.

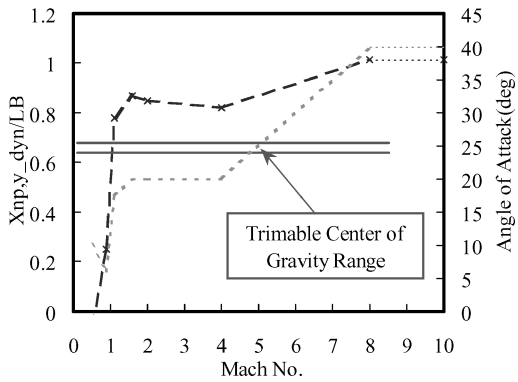

Fig. 21 Lateral/directional static stability of the baseline configuration.

On the other hand, the adjustment to the cant angle of the baseline configuration from 20 to 45 deg is a modification that not only shifts neutral point aft but also the center of pressure, as described earlier. Because the relatively aft location of the trimable center of gravity range is one of cause of the instability, this adjustment is unfavorable for the baseline configuration.

Fin-off modification is somewhat more effective than cant-angle modification, because it has shifted the center of pressure forward especially at transonic and low supersonic speeds. Furthermore, because the baseline configuration has relatively large $Cm\alpha$ at transonic speeds as a result of the nonlinear characteristics (Fig. 6), fin-off configuration has shown to be somewhat better on longitudinal stability. However, the fin-off modification generally produces an unstable effect, and its improvement is actually not sufficient for the baseline configuration.

Lateral/Directional Static Stability

Lateral/directional static stability for the baseline configuration at nominal angles of attack with varying Mach number is shown in Fig. 21 in terms of $Xnp,y\_dyn/LB$, which is defined as

$$Xnp,y\_dyn/LB = \{Xcg - Cn\beta dyn \times b/CY\beta/\cos\alpha\}/LB \qquad (1)$$

where $CY\beta$ is the side-force coefficient derivative and $Cn\beta dyn$ is given as

$$Cn\beta dyn = Cn\beta \times \cos\alpha - Izz/Ixx \times Cl\beta \times \sin\alpha \qquad (2)$$

Considering the similarity between the configurations of the present vehicle and the HL-20,[11] Izz/Ixx for the present vehicle was assumed as five. $Cn\beta dyn$ can be interpreted as a coefficient representing directional stability in the stability axis system, and $Cn\beta dyn > 0$ means that the vehicle is stable as a whole in lateral and directional motions. Therefore, similar to the neutral point in longitudinal stability,

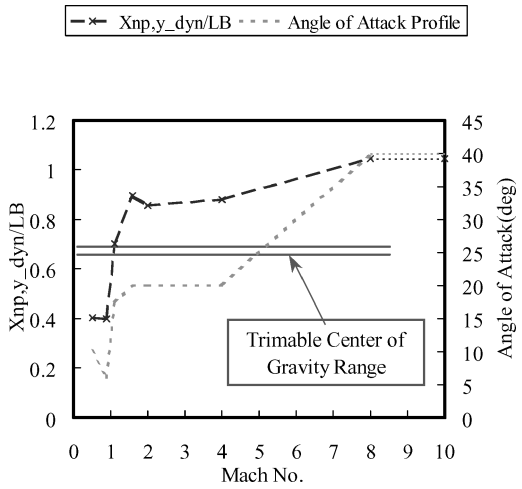

Fig. 22 Lateral/directional static stability of the 45-deg canted-fin configuration.

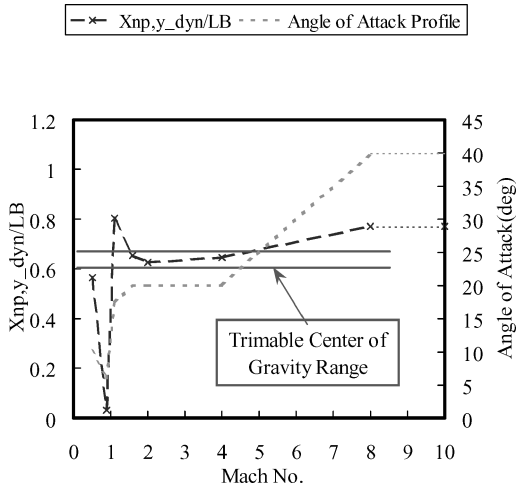

Fig. 23 Lateral/directional static stability of the fin-off configuration.

the vehicle is laterally and directionally stable as a whole when Xnp, y_dyn/LB is aft of the center of the gravity.

The trimable center-of-gravity range from Fig. 16 is also show in Fig. 21 for comparison. $Xnp,y\_dyn/LB$ is aft of the trimable center-of-gravity range at $M > 1$; therefore, the baseline configuration is laterally and directionally stable when $M > 1$ but unstable at $M < 1$. The unstable characteristics at $M < 1$ are caused by the nonlinear characteristic shown in Figs. 7 and 8.

Lateral/directional static stability with varying Mach number for the 45-deg canted-fin configuration and fin-off configuration are shown in Figs. 22 and 23, respectively, in terms of $Xnp,y\_dyn/LB$ at nominal angles of attack. The trimable center-of-gravity ranges from Figs. 17 and 18 are also show for comparison. Similar to the baseline configuration, the 45-deg canted-fin configuration becomes unstable at $M < 1$. $Xnp,y\_dyn/LB$ of the fin-off configuration is forward of that of the baseline configuration but is either aft of or within the trimable center-of-gravity range at $M > 1$ and unstable at $M < 1$. The fin-off configuration is not totally unstable as a whole laterally and directionally because of the relatively high angle-of-attack profile, which makes dihedral characteristics $Cl\beta$ more stable and effective on $Cn\beta dyn$. Therefore the fin-off configuration can be laterally/directionally stable if it flies at relatively high angles of attack, at least at supersonic speeds.

Figure 24 shows the lateral/directional static stability with varying Mach number for the upswept upper-aftbody configuration in terms of $Xnp,y\_dyn/LB$ at nominal angles of attack. The trimable center-of-gravity range from Fig. 19 is also shown for comparison. $Xnp,y\_dyn/LB$ is aft of the trimable center-of-gravity range at all Mach numbers, and so the upswept upper-aftbody configuration is

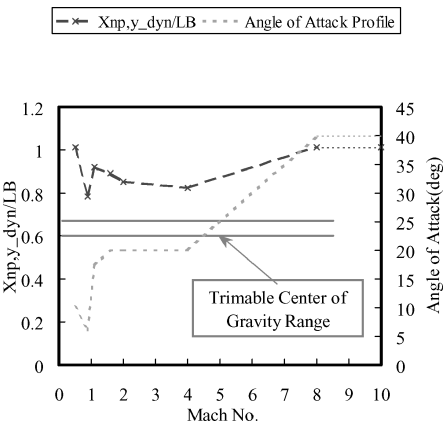

Fig. 24 Lateral/directional static stability of the upswept upper-aftbody configuration.

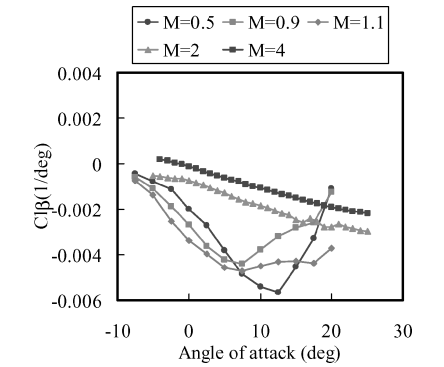

Fig. 25 Rolling-moment coefficient of the upswept upper-aftbody configuration.

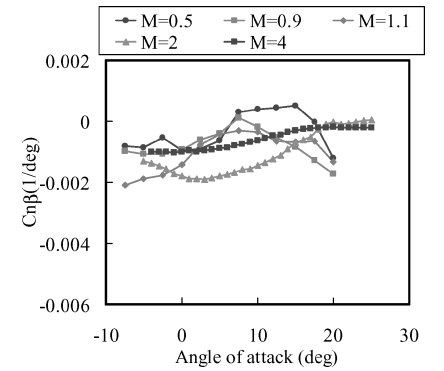

Fig. 26 Yawing-moment coefficient of the upswept upper-aftbody configuration.

laterally and directionally stable over the whole flight Mach-number range.

The upward deflection of the upper-aft surface of the fuselage is most effective mainly because of the following reasons. The most effective approach to improve the lateral/directional stability of the baseline configuration is to improve the directional stability at $M < 1$. Such an improvement can be realized by reducing the instability produced by the vortex like flow at the upper-aft surface of the fuselage. One approach to prevent such a flow is to raise the pressure at the upper-aft surface of the fuselage, which can be realized by the upward deflection. As can be seen by comparing Figs. 25 and 26, which shows the $Cl\beta$ and $Cn\beta$ of the upswept upper-aftbody configuration respectively, with Figs. 7 and 8, the lateral/directional stability has improved on the upswept upper-aftbody configuration at $M < 1$. Other modifications basically have an unstable effect on directional stability and are not favorable in terms of improving the lateral/directional stability of the baseline configuration.

The preceding discussions and the discussions in the preceding section suggest that modification of the upper-aft part of the fuselage

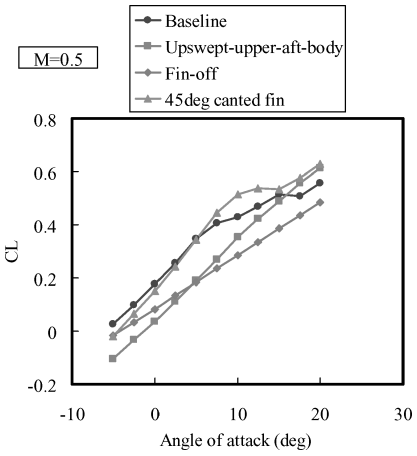

Fig. 27 Lift coefficient at $M = 0.5$ for four configurations.

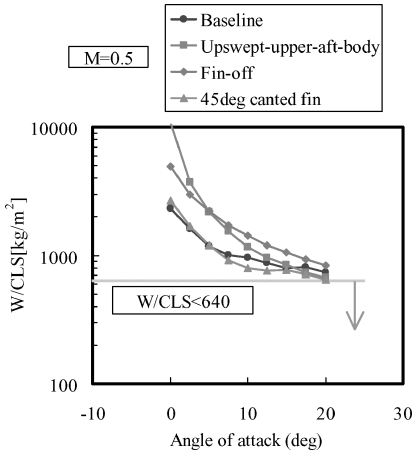

Fig. 28 *W/CLS* at $M = 0.5$ for four configurations.

seems to be the most promising approach in terms of improving longitudinal trim and longitudinal and lateral/directional stability. More sophisticated modification of the upswept shape can lead to fully meeting the requirement to maintain both trim and static stability.

Subsonic Lifting Surface Loading

Subsonic lift or lifting surface loading W/CLS at subsonic speed is a key characteristic for vehicle recovery of the current concept because it is related to parachute or parafoil deployment. The target W/CLS was tentatively set at 640 kgf/m^2 or below based on the X-38 pilot parachute deployment condition.[12]

Figure 27 shows the lift coefficient of the four configurations at $M = 0.5$, and Fig. 28 shows the W/CLS at $M = 0.5$ for the same configurations based on the estimated vehicle weight. As Fig. 28 shows, none of the four configurations reaches the target value even at the highest angle of attack tested (20 deg) because of either the nonlinear lift-curve characteristics of the baseline and 45-deg canted-fin configurations or the intrinsically low lift of the fin-off and upswept upper-aftbody configurations, as can be seen from Fig. 27. Therefore some improvement of lift characteristics is necessary, but also further investigation of the target value of W/CLS itself is necessary for further analysis.

Conclusions

Transonic and supersonic wind-tunnel tests to investigate the aerodynamic characteristics of lifting-body-type reentry vehicle configurations were conducted at NAL's 2 m × 2 m Transonic Wind Tunnel and 1 m × 1 m Supersonic Wind Tunnel. Test results indicated unfavorable nonlinear characteristics for the baseline configuration, which is caused by flow separation induced by the outboard fins.

Longitudinal trim capability and longitudinal static stability of the four configurations, namely, the baseline configuration, a 45-deg canted-fin configuration, a fin-off configuration, and an upswept upper-aftbody configuration, were compared. Although none of the configurations is statically stable throughout the entire flight Mach-number range from subsonic to hypersonic, the upswept upper-aftbody configuration is mostly stable and has a relatively wide trimable center-of-gravity range. This is caused by the forward shift of center of pressure at transonic and low supersonic speeds resulting from the upward deflection of the upper aft surface.

The lateral/directional stability of the four configurations was also compared. The upswept upper-aftbody configuration demonstrated good lateral/directional stability. Modifying the upper-aft part of the fuselage of the baseline configuration therefore appears to be the most promising approach to improving its characteristics, and further modification of the upswept shape can lead to fully stable characteristics.

Comparison of the subsonic lifting surface loading W/CLS for the four configurations found that no configuration reached the target value. Further investigation of the W/CLS target value is necessary.

Acknowledgments

The authors acknowledge the staff of the 2 m × 2 m Transonic Wind Tunnel and the 1 m × 1 m Supersonic Wind Tunnel of the National Aerospace Laboratory of Japan for their efforts in the wind-tunnel tests. The authors also acknowledge T. Tsujimoto of the National Space Development Agency of Japan and staff of the Flight Testing Technology Group at National Aerospace Laboratory's Space Transportation Project Center, among those that are not under the joint signatures of the present paper, for their support in the wind-tunnel tests.

References

[1]Akimoto, T., Ito, T., Yamamoto, M., Bando, T., and Inoue, Y., "Orbital Re-Entry Experiment (OREX)—First Step of Space Return Flight Demonstrations in Japan," International Astronautical Federation, Paper IAF-94-V.2.525, Oct. 1994.

[2]Shirouzu, M., and Yamamoto, M., "Overview of the HYFLEX Project," AIAA Paper 96-4524, Nov. 1996.

[3]Nagayasu, H., and Nagayasu, M., "On the Automatic Landing Flight Experiment (ALFLEX)," National Aerospace Lab. of Japan, NAL SP-39T, Tokyo, Aug. 1998.

[4]Miyazawa, Y., Yanagihara, M., Sarae, W., Akimoto, T., Cretenet, J. C., and Bonnal C., "HOPE-X High Speed Flight Demonstrator Research Program," Japan Society for Aeronautical and Space Science and 22nd ISTS Organization Committee, 22nd International Symposium on Space Technology and Science, Paper 2000-g-19, Tokyo, May–June 2000.

[5]Fujii, K., Tsuchiya, T., Kai, T., Ito, T., Watanabe, S., Nakamura, T., Ishimoto, S., Kawato, H., Nishiwaki, K., and Shirouzu, M., "Concepts of Reentry Technology Experimental Vehicles," AIAA Paper 2002-5264, Sept.–Oct. 2002.

[6]Barret, C., "The Lifting Body Legacy—X-33," AIAA Paper 99-0382, Jan. 1999.

[7]Kochiyama, J., Tsujimoto, T., and Shirouzu, M., "Current Status of the H-II Orbiting Plane-Experimental (HOPE-X) Development," Japan Society for Aeronautical and Space Science and 22nd ISTS Organization Committee, 22nd International Symposium on Space Technology and Science, Paper 2000-g-6, Tokyo, May–June 2000.

[8]Woods, W. C., Arrington, J. P., and Hamilton, H. H., II, "A Review of Preflight Estimates of Real-Gas Effects on Space Shuttle Aerodynamic Characteristics," *Shuttle Performance: Lessons Learned*, NASA CP-2283, Pt. 1, 1983, pp. 309–346.

[9]Watanabe, S., Kawato, H., Fujii, K., Yamamoto, Y., and Ogasawara, K., "An Experimental Investigation on Subsonic to Supersonic Aerodynamic Characteristics of a Lifting-Body-Type Reentry Vehicle," Japan Society for Aeronautical and Space Science and 23rd ISTS Organization Committee, 23rd International Symposium on Space Technology and Science, Paper 2002-g-12, Tokyo, May 2002.

[10]Tsujimoto, T., Sakamoto, Y., Akimoto, T., Kouchiyama, J., Ishimoto, S., and Aoki, T., "Aerodynamic Characteristic of HOPE-X Configuration with Twin Vertical Tails," AIAA Paper 2001-1827, April 2001.

[11]Powell, R. W., "Six-Degree-of-Freedom Guidance and Control-Entry Analysis of the HL-20," *Journal of Spacecraft and Rockets*, Vol. 30, No. 5, 1993, pp. 537–542.

[12]Smith, J., Bennett, T., and Fox, R., "Development of the NASA X-38 Parafoil Landing System," AIAA Paper 99-1730, June 1999.

W. Williamson
Associate Editor